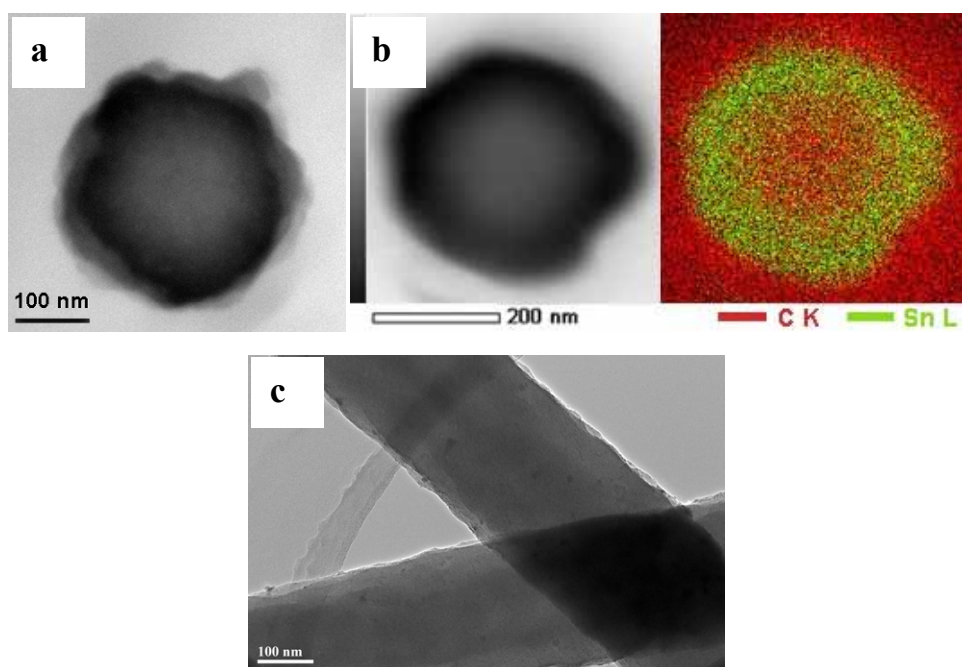


## Supporting information

### Carbon/SnO<sub>2</sub>/Carbon Core/Shell/Shell Hybrid Nanofibers: Tailored Nanostructure for Anode of Lithium Ion Batteries with High Reversibility and Rate Capacity

Junhua Kong, Zhaolin Liu, Zhengchun Yang, Hui Ru Tan, Shanxin Xiong, Siew Yee Wong,  
Xu Li\* and Xuehong Lu\*



**Fig. S1.** (a) Cross section TEM image of the carbon/SnO<sub>2</sub> (HF50) hybrid nanofibers, showing the core/shell morphology with carbon-rich core of approximately 200 nm in diameter and SnO<sub>2</sub>-rich shell of about 50 nm in thickness. (b) Scanning TEM-energy dispersive X-ray spectroscopy (STEM-EDX) element mapping image of HF50, confirming the formation of carbon/SnO<sub>2</sub> core/shell morphology after carbonization. (c) TEM side view of HF50, showing the compact SnO<sub>2</sub> shell with relatively smooth surface.

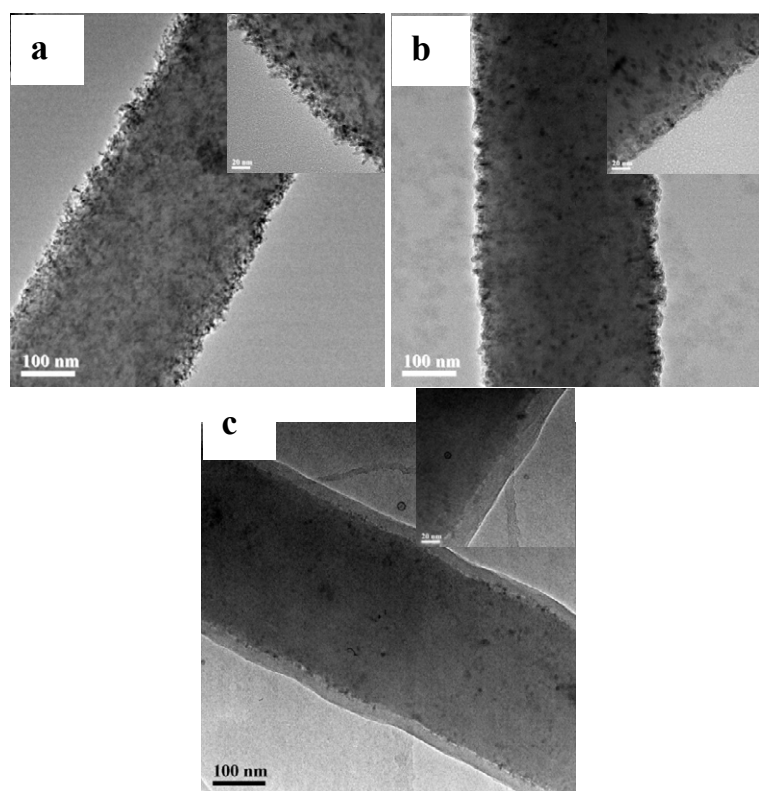


**Fig. S2.** TEM side views of carbon/SnO<sub>2</sub>/carbon core/shell/shell hybrid nanofibers with carbon skin in various thicknesses through adjusting the glucose concentration from (a) 1 mg/ml, (b) 2.5 mg/ml, (c) 10 mg/ml. Insets show the corresponding high magnification images. The thickness of carbon skin increases with increase of glucose content. The roughness of surface of SnO<sub>2</sub> shell and appearance of carbon-embedded distinguishable SnO<sub>2</sub> nanoparticles with size of less than 10 nm can be clearly observed, which is due to the high-pressure and high-temperature hydrothermal treatment for long time. The surface of deposited carbon skin is smooth.

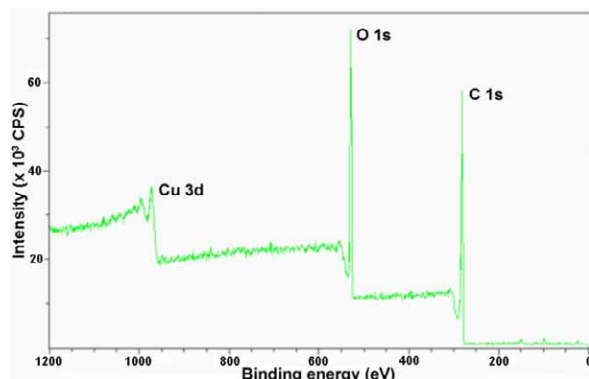


**Fig. S3.** XPS result of BP-HF50/C15 collected from hydrothermal mother solution of HF50/C15. No obvious signal can be assigned to Sn (at binding energy of 493.2 eV for Sn 3d<sup>3/2</sup>) in XPS spectrum, indicating that SnO<sub>2</sub> is not dissolved into solution during hydrothermal treatment.

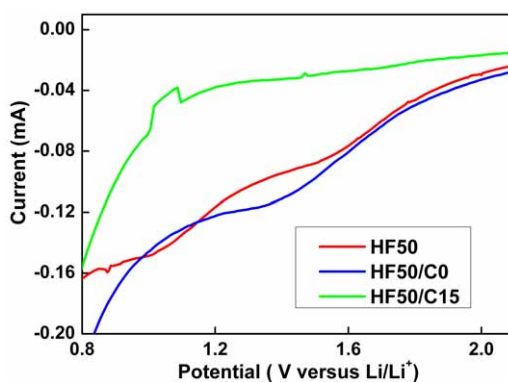


**Fig. S4.** Enlarged cyclic voltammograms of HF50, HF50/C0 and HF50/C15 at the 1st cycle between the voltage window and scanning rate of 2.1~0.8 V and 0.01 mV/s, respectively. The broad reduction peak at 0.8~1.7 V can be clearly observed.

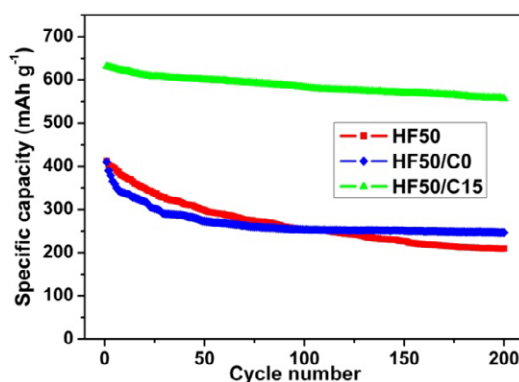


**Fig. S5.** Cycle capacity of HF50, HF50/C0 and HF50/C15 at charging rate of 1C. The cycling test condition is as follows: discharging at 1C rate to 0.005V, then standby for 5 min, and finally discharging at 0.1C rate to 0.005V followed by charging at 1C rate to 3V.

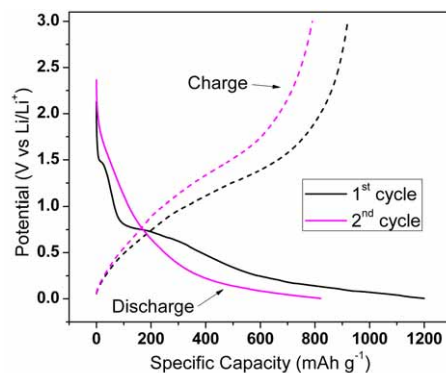


**Fig. S6.** Discharge/charge profile (1<sup>st</sup> and 2<sup>nd</sup> cycle) of pure carbon nanofibers with hydrothermally coated carbon skin of 15-nm thickness. Hydrothermal treatment and post calcination was carried out to the pure carbon nanofibers under the same conditions as that for HF50/C15. The capacity test at current rate of 0.1C was carried out under following conditions: discharging at 1C rate to 0.005V, then standby for 5 min, and finally discharging at 0.2C rate to 0.005V followed by charging at 0.1C rate to 3V. Higher capacity than that of graphite is observed for this reference sample.

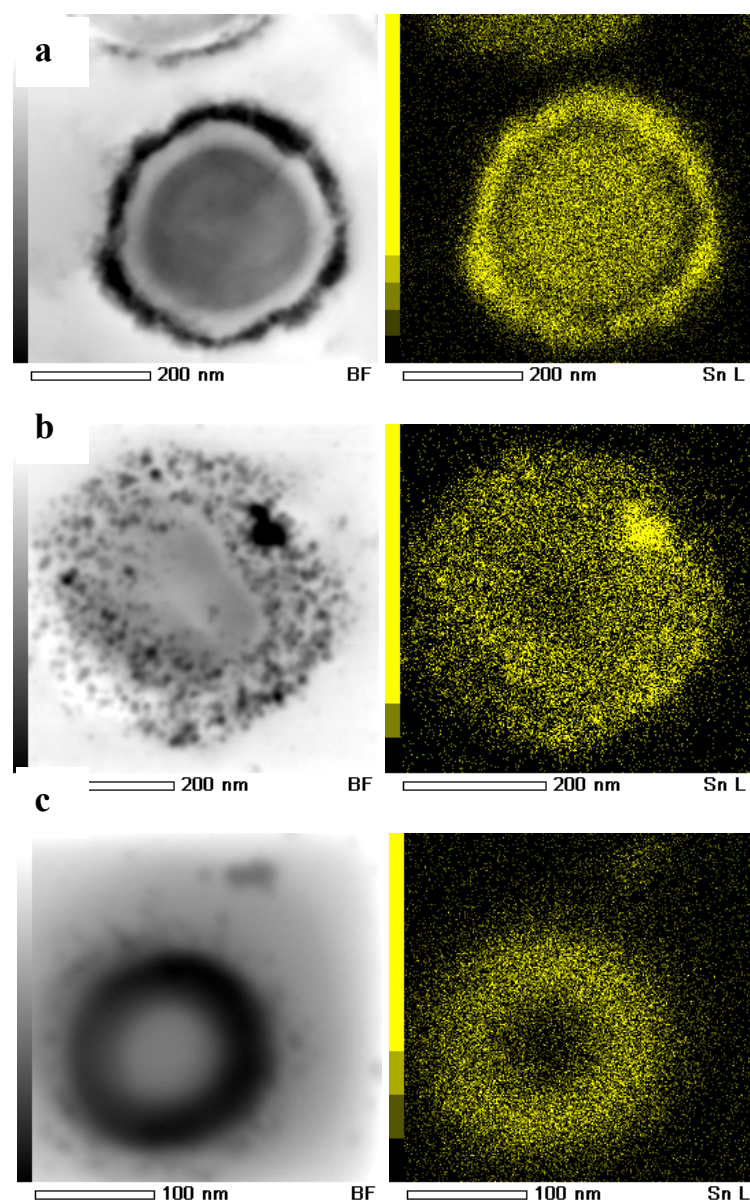


**Fig. S7.** STEM-EDX element mapping of (a) HF50, (b) HF50/C0 and (c) HF50/C15 after 50 charging cycles at current rate of 0.1C, showing the morphology change after discharge/charge. It is clearly showed that detachment occurred for HF50 after cycling, resulting in a wide gap between carbon core and SnO<sub>2</sub> shell, which is due to the outward expansion of SnO<sub>2</sub>. This expansion is also observed in HF50/C0, in which the SnO<sub>2</sub> shell

became very loose, and individual SnO<sub>2</sub> nanoparticles turned to be larger due to the aggregation during discharge/charge. In contrast, the core/shell/shell morphology of HF50/C15 is well preserved after cycling, indicating the excellent stability of the designed structure.